Article

Dynamic Monitoring of MicroRNA-DNA Hybridization Using DNAase-Triggered Signal Amplification

Xiaopei Qiu, Xing Liu, Wei Zhang, Hong Zhang, Tianlun Jiang, Dongli Fan, and Yang Luo

Anal. Chem., **Just Accepted Manuscript** • DOI: 10.1021/acs.analchem.5b01159 • Publication Date (Web): 12 May 2015

Dynamic Monitoring of MicroRNA-DNA Hybridization Using DNAase-Triggered Signal Amplification

Xiaopei Qiu[#†], Xing Liu[#‡], Wei Zhang[# §], Hong Zhang[†], Tianlun Jiang[†], Dongli Fan[‡], Yang Luo[*†]

[†]Department of Blood Transfusion Medicine, Southwest Hospital, the Third Military Medical University, Chongqing 400038, China. [‡]Department of Plastic Surgery, Xinqiao Hospital, the Third Military Medical University, Chongqing 400037, China. [§]Chongqing Institute of Green and Intelligent Technology, Chinese Academy of Sciences, Chongqing 400714, PR China. [#]These authors contributed equally.

[*]E-mail: luoyang@tmmu.edu.cn. Tel.: 86-23-68765485. Fax: 86-23-68765986.

ABSTRACT: Dynamically monitoring microRNA (miRNA)-DNA reactions is critical for elucidating various biological processes. However, traditional strategies fail to capture this dynamic event because the original targets are pre-amplified. In the present study, we developed an amplification-free strategy for real-time monitoring of miRNA-DNA hybridization that integrates the advantages of both duplex-specific nuclease (DSN)-triggered signal amplification and single-stranded DNA probe coating facilitated by reduced graphene oxide. DSN-mediated miRNA recognition was found to consist of two phases: hybridization and hybridization-cleavage. In the presence of miRNA and DSN, hybridization of a 22-mer miRNA-DNA could be completed within 7 min by observing the angle increase in a surface plasmon resonance (SPR) biosensor. The subsequent hybridization-cleavage process could be visualized as a gradual SPR angle decrease that occurred until all coated probes were hydrolyzed. In addition, for miRNA-21 detection, the proposed linear signal amplification assay demonstrated a sensitivity of 3 fM over a dynamic range of 5 orders of magnitude.

A microRNA (miRNA) molecule is a small non-coding RNA molecule with a length of approximately 22 nucleotides that functions in RNA silencing and post-transcriptional regulation of gene expression. Recently, miRNAs have been found to have tremendous potential as diagnostic biomarkers due to their roles in modulating carcinoma development.[1] Circulating miRNA (cmiRNA), an miRNA that is present in various biological fluids, is particularly attractive due to its potential as a diagnostic and prognostic biomarker, which stems from its remarkably increased resistance to digestion by ribonucleases and degradation by repeated freeze-thaw cycles.[2-4] Because cmiRNA is present at very low concentrations, rapid and highly sensitive profiling of trace cmiRNA is challenging.[5,6]

There are currently three main approaches to miRNA determination: quantitative reverse transcription polymerase chain reaction (qRT-PCR),[7,8] hybridization-based methods, and high-throughput sequencing.[9] The qRT-PCR approach offers sufficient sensitivity, down to the nanogram level, for total RNA. However, a hurdle in performing highly parallel qRT-PCR is that the optimal reaction conditions may vary substantially among miRNAs due to sequence-specific differences in primer annealing. In addition, the performance of most of the recently developed assays depends strictly on the use of locked nucleic acid (LNA)-modified primers, which significantly increases the detection cost.[10,11] Microarray-based hybridization is particularly effective for profiling large numbers of miRNAs because of its low cost and high-throughput capability,[12] but the difficulty of obtaining melting temperature-normalized probe sets for genome-wide expression profiling must be overcome.[13,14] Finally, high-throughput sequencing is advantageous for profiling the miRNAs of both novel and known miRNAs and for identifying miRNA sequences precisely. However, the results of sequencing may vary in terms of adapter and primer sequences, and bias can be introduced at various steps of miRNA detection, such as linker ligation, reverse transcription, or PCR amplification.[15] More importantly, an in vitro target amplification procedure is required in all of the above-mentioned assays to exponentially amplify the initial target nucleic acid molecules, making real-time monitoring of the miRNA-DNA hybridization process impractical.

Recently, duplex-specific nuclease (DSN) with DNAase activity has been exploited to mediate an amplification-free strategy for miRNA detection because of its strong preference for hydrolyzing DNA in DNA-RNA heteroduplexes, rather than in single-stranded (ss) DNA or RNA.[16,17] The analytical specificity has been significantly improved in DSN-mediated analytical strategies because the risk of nonspecific amplification can essentially be eliminated.[18-22] However, to the best of our knowledge, no existing miRNA quantification approaches have elucidated the dynamic processes of miRNA-DNA hybridization as well as the DSN-induced cleavage of the induced hybrid.

Herein, we developed a DSN-coupled surface plasmon resonance (DSN-SPR) approach for label-free and ultrasensitive determination of cmiRNA. Notably, the dynamic behavior of miRNA-DNA hybridization and DSN cleavage has been monitored using this proposed assay. Ultrasensitive recognition of cmiRNA was achieved by integrating the advantages of DSN-mediated isothermal signal amplification and the high adsorption capability of reduced graphene oxide (rGO) in coating oligonucleotide probes with SPR biosensor-associated real-time monitoring.

EXPERIMENTAL SECTION

Materials and apparatus. HPLC-purified SH-labeled DNA probes and miRNAs (Table 1) and 10× TBE powder (0.089 M Tris, 0.089 M boric acid, and 0.002 M EDTA) were purchased from Sangon Biotech (Shanghai, China). A DSN kit containing 100 U DSN and 10× DSN master buffer (50 mM Tris-HCl, pH 8.0) was obtained from Evrogen (Moscow, Russia). SYBR Green II, RNase inhibitor, salmon sperm DNA, a 20 bp DNA ladder and 6× loading buffer were obtained from Invitrogen (Shanghai, China). Agarose gels, PBS, Na_2SO_4, H_2SO_4 and all other chemicals were of analytical reagent grade and were purchased from Sigma (St. Louis, MO). Ultrapure water (18.2 MΩ) obtained from a Milli-Q Integral water purification system (Darmstadt, Germany) was used throughout the study. A graphene oxide (GO) stock solution (3.0 mg/mL) was purchased from SinoCarbon™ (Shangxi, China). All experiments involving miRNA were carried out in an RNase-free environment. The tips and tubes used were also RNase free and did not require pretreatment to inactivate RNases. All buffer solutions were treated with 0.1% DEPC and autoclaved.

Table 1. Sequences of DNA probes and miRNAs used in this work

Name	Sequence (5'–3')	Length (nt)
P-21 (P_1)	ATCGAATAGTCTGACTACAACT	22
P-21 (P_2)	SH-ATCGAATAGTCTGACTACAACT	22
P-7b (P_3)	ACTCCATCATCCAACACACCAA	22
miR-21 (T_1)	UAGCUUAUCAGACUGAUGUUGA	22
miR-141 (T_2)	UAACACUGUCUGGUAAAGAUGG	22
miR-143 (T_3)	UGAGAUGAAGCACUGUAGCUCA	22
let-7a (T_4)	UGAGGUAGUAGGUUGUAUAGUU	22
let-7b (T_5)	UGAGGUAGUAGGUUGUGUGGUU	22
let-7c (T_6)	UGAGGUAGUAGGUUGUAUGGUU	22
let-7e (T_7)	UGAGGUAGGAGGUUGUAUAGU	21

The SPR instrument used was a UMPHO™ A600 from CytoTrend (Beijing, China) with an excitation wavelength of 650 nm. A 20 mm × 28.6 mm sensor chip coated with a 50 nm-thick gold layer on the silicon substrate was supplied by CytoTrend (Beijing, China). A real-time PCR detection system from Bioneer (Shanghai, China) was utilized for PCR amplification. Electrophoresis was performed using a Hema GSG-2000 gel imaging system equipped with a 13 M CCD from Mingmei (Guangzhou, China). The data were analyzed using SPSS 20.0 software (SPSS Inc. Chicago, IL), and fitting

of the experimental data was accomplished using Origin software (version 9.0).

Electrophoretic deposition of rGO onto gold-based SPR chips. A GO working solution (0.5 mg/mL) was prepared by diluting the GO stock solution in a 0.1 M Na_2SO_4 solution, followed by ultrasonication for 3 h to obtain a homogeneous brown solution. Electrophoretic deposition of the rGO was then carried out using cyclic voltammetry (CV; -1.24 to 0.76 V vs reversible hydrogen electrode [RHE], 50 mV s^{-1}) in the GO working solution in a standard three-electrode cell. Hg/HgO and platinum (Pt) sheets served as the reference and counter electrodes, respectively, and the SPR interface (Au/silicon prism) substrate served as the working electrode. These three electrodes were placed parallel to each other in the GO working solution at intervals of 1 cm, and the deposition procedure was not terminated until the CV curves were reproduced up to 500 times. After deposition, the interface was washed three times using deionized water, followed by blow-drying with nitrogen.

Optimization of coated probe concentrations. DNA probes were deposited on the surface of the rGO sensor chip via π-stacking interactions.[23] The total volume of the coating solution was 50 μL, comprising 35 μL of loading buffer and 15 μL of probe. The DNA probes were specifically deposited on the surface of the rGO sensor chip at concentrations ranging from 1 μM to 30 μM at 25°C for 60 min. The probe-coated rGO chip was then rinsed thoroughly with PBS (0.15 M NaCl and 10 mM phosphate, pH 7.2) to remove any uncoated oligonucleotide probes. Next, the rGO chip was incubated with 2 mg/mL salmon sperm DNA solution for 30 min to block any naked/bare sites on the rGO interface, preventing nonspecific adsorption. The sensing interface, denoted as the rGO/probe, was obtained after thoroughly washing the modified SPR chip with PBS (0.15 M NaCl and 10 mM phosphate, pH 7.2).

miRNA detection procedure. The target miRNAs were detected in the SPR biosensor at an excitation wavelength of 650 nm by recording the SPR angle shifts in real time. The working mixture contained 1× DSN master buffer, 0.2 U DSN, hybridization buffer (0.15 M NaCl, 0.3 M KCl, 10 mM phosphate, and 0.005% Tween 20, pH 7.2), 10 U RNase inhibitor, ultrapure water and target miRNAs. During detection, 50 μL of the working mixture was pipetted into the detection well and allowed to repeatedly hybridize and cleave at 50°C for 60 min (the longest time feasible in the current experimental setting because a prolonged hybridization time would lead to an undesired SPR waveform change due to evaporation of the working solution). A thorough rinse using PBS was then applied to terminate the detection procedure.

Operating characteristics. An miRNA-21 (miR-21) stock solution (100 μM) was prepared by dissolving miR-21 in dry powder form in TE buffer (10 mM/L Tris-HCl and 1 mM/L EDTA, pH 8.0). Calibration standards were prepared by diluting the miR-21 stock solution to achieve a series of different concentrations (0.01, 0.1, 1, 10, and 100 pM). The sensitivity of the proposed detection assay was then determined by measuring the SPR angle shifts for the serially diluted miR-21 calibrators and plotting the measured shifts as a function of the miR-21 concentration. The specificity of the assay was also tested by detecting different targets (miR-21, miR-141, and miR-143) using an miR-21 probe-coated rGO chip and detecting let-7b, let-7a, let-7c and let-7e using a let-7b probe-coated rGO chip.

Clinical sample detection and methodology comparison. In total, 104 clinical blood samples were collected from individuals at Southwest Hospital, which is affiliated with the Third Military Medical University. Among these samples, 17 were from liver cancer inpatients, 22were from colorectal cancer inpatients, 19 were from gastric cancer inpatients, 22 were from lung cancer inpatients, and 24 were from breast cancer inpatients (average age of 58.4 years), as confirmed using immunochemistry. Another 20 samples from healthy individuals (average age of 52.8 years) were selected as controls. This study was approved by the Ethics Board of the Third Military Medical University. All peripheral venous blood samples were collected in BD Vacutainer tubes (Franklin Lakes, NJ) and then centrifuged at 3000 rpm for 10 min. The serum was immediately separated, frozen and stored at -80°C until detection and analysis, with no freeze-thaw cycles.

The total RNA, including miRNAs, was extracted from the peripheral venous serum using the miRNeasy Serum/Plasma Kit from Qiagen (Hilden, Germany) according to the manufacturer's instructions. The pure and concentrated RNA was then divided into two equal parts for detection using the proposed DSN-SPR assay or qRT-PCR. To deactivate or solubilize proteins that might inhibit the qRT-PCR, we mixed 2.5 μL of each serum sample with 2.5 μL of a preparation buffer containing 2.5% Tween 20, 50 mmol/L Tris, and 1 mmol/L EDTA. RNA was reverse transcribed into cDNA using an AMV First-Strand Synthesis Kit from Sangon Biotech (Shanghai, China) according to the manufacturer's instructions. The transcribed cDNA was then used as the template for qRT-PCR.

The primers for miR-21 amplification were 5'-GCCCGCTAGCTTATCAGACTGATG-3' (forward) and 5'-GTGCAGGGTCCGAGGT-3' (reverse). Real-time PCR was performed to measure the expression levels of target miRNAs using the QuantiTect™ SYBR® Green PCR Kit from Qiagen (Hilden, Germany) according to the manufacturer's instructions. RNU6B was used as the reference control for tissue studies, and miR-16 (5'-UAGCAGCACGUAAAUAUUGGCG-3') was used as the reference control for the serum studies.

RESULTS AND DISCUSSION

Assay principle. As illustrated in Figure 1, the proposed DSN-SPR assay quantifies the original target concentration by capturing the linearly amplified raw SPR signal from the target miRNA. In the presence of target miRNA, the ssDNA probe immobilized on the surface of the rGO SPR chip hybridizes to the target to form an miRNA-DNA hybrid, which in turn serves as a substrate for DSN cleavage. Because the DSN only cleaves the ssDNA oligonucleotide in the context of an miRNA-DNA duplex, the target miRNA could be released upon cleavage and re-hybridize to the remaining ssDNA probe, initiating another round of cleavage, release,

and hybridization. In a system with sufficient DSN, the target miRNA and DSN would react repeatedly, allowing linear amplification of the original SPR angle shift signal in real time until all of the immobilized ssDNA probes are cleaved.

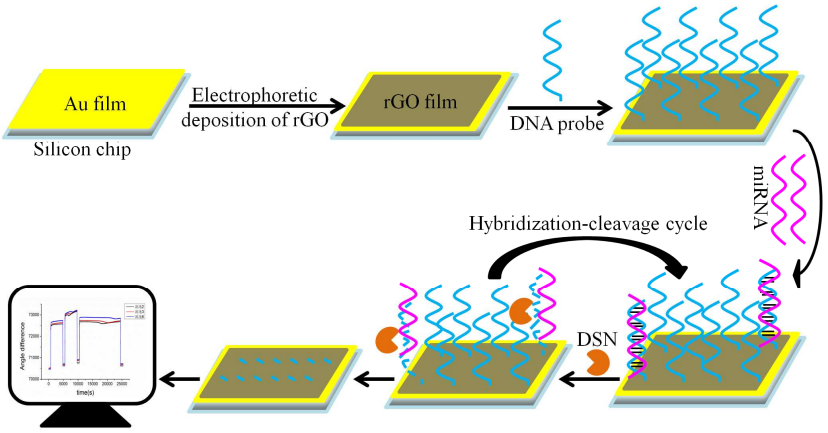

Figure 1. Schematic diagram of the proposed DSN-SPR assay. The ssDNA probe was immobilized on the surface of the rGO-modified SPR biosensor. After introducing both the target miRNA and DSN into the biosensor, a hybridization-cleavage cycle was initiated to induce linear signal amplification of the raw SPR angle shift, allowing the target miRNA to be quantified in real time.

Real-time monitoring of miRNA-DNA hybridization and DNA cleavage. miR-21 was selected as the model to demonstrate the proposed monitoring platform because this miRNA is a prevalent cmiRNA biomarker that is overexpressed in various human cancers.[24-26] An ssDNA probe (P-21) complementary to miR-21 was prepared and immobilized on the SPR chip to capture the target miR-21. The signal amplification process could be monitored continuously as the number of hybridization-cleavage cycles increased. The presence of miR-21 led to an obvious increase in the SPR angle, suggesting successful hybridization between miR-21 and its corresponding ssDNA probe (Figure 2a). The occurrence of hybridization was validated by a negligible SPR angle shift in the absence of the target miR-21, regardless of the presence of DSN. However, in the presence of both the target miR-21 and DSN, the SPR angle shift increased promptly and then gradually decreased until reaching an endpoint. These results reflected the dynamic process of miRNA detection using the proposed DSN-SPR assay, which comprises two stages: a hybridization stage and a hybridization-cleavage stage. The hybridization stage occurs when the target miRNA is introduced and ends when the SPR angle shift peaks. The hybridization-cleavage stage is initiated when the miRNA-DNA hybrid is completely formed; the ongoing hybridization-cleavage step will then induce a gradual decrease in the SPR angle until the end of the stage, at which point all of the coated probes have been cleaved.

We observed that the entire hybridization process between miR-21 and the P-21 probe could be completed within 7 min under optimal hybridization conditions (Figure 2a). In this study, the miRNA solution with the lowest target density (10 fM) was employed to reflect the miRNA-DNA hybridization on the outset layer of the coated probe array because trace miRNA molecules preferentially hybridize to the peripheral ssDNA probe on the chip. The electrostatic repulsion between the target and the underlying probe as well as the repulsion between probes has been reported to be stronger in the middle of the probe array than at the edge of the chip.[27] In the current study, the SPR angle increased promptly in the first 60 sec of sampling, after which it increased slowly before reaching a plateau within 7 min. The angle then decreased gradually until the end of the cleavage process. As reported in previous studies,[28,29] in a bulk solution, the RNA-DNA hybridization process involves two phases: a fast phase and a slow phase. These phases are characterized by two distinct increasing trends in the SPR angle. Previous diffusional fluorescence correlation analysis also revealed that RNA-DNA hybridization was a biphasic, irreversible second-order reaction in which the first phase could be completed very quickly (several seconds to minutes), whereas the second phase was remarkably long (sometimes over several hours).[30] In our experiments, a very short duration (< 7 min) was needed to complete the two-phase hybridization procedures, which is shorter than that reported previously. Several factors may contribute to this rapid detection, including differences in the hybridization parameters and probe length as well as the only partial completion of the second phase of hybridization. Considering that the influence of hybridization may not be particularly significant, we postulated that the proposed SPR assay was unable to fully characterize the slow phase of hybridization. Similar phenomena have been previously reported by showing that SPR can only characterize the detected duplex nucleation or initial target recognition.[28,31] Based on these observations, it could be concluded that DSN-mediated cleavage of an miRNA-DNA duplex can be initiated despite the hybridization not being fully completed.

Importantly, the cleavage stage dynamically reflects the simultaneous processes of both hybridization and cleavage. The decrease in SPR angle observed in the present study, reflecting the effect of hybridization, was overwhelmed by the hydrolysis of the coated ssDNA probe, and it was extremely difficult to distinguish between the two processes in a bulk solution. As Figure 2b illustrates, the DSN-mediated cleavage activity could be further verified by agarose gel electrophoresis, by which the target miRNA (lane 4), the ssDNA probe (lane 5), and the miRNA-DNA hybrid (lane 2)

could be clearly observed in the absence of the DSN enzyme. Meanwhile, the P-21 probe band was absent, and only the miR-21 band could be observed in the DSN-cleaved product (lane 1), confirming successful hydrolysis of the DNA strand in the miRNA-DNA complex.

As reported by previous studies on hybridization kinetics, major factors contributing to the interfacial binding process are the ionic strength and pH of the buffer solution, the temperature, the sequence length[32] and the chemical nature of the base units.[33] In actual analytical practice, the hybridization parameters are pre-optimized prior to detection, and the target length and the molecular structure of the sequence are varied according to the target biomolecules. In the present study, considering that the sequence lengths of most miRNAs are identical, two 22-mer-length miRNAs (miR-21 and let-7b) with different oligonucleotide compositions were analyzed to reveal the influence of the sequence composition on the hybridization rate. It was observed that the hybridization rate between P-21 and miR-21 (6.05 min) was slightly higher than the rate between P-7b and let-7b (7.1 min) (Figure 2c), reflecting distinct hybridization kinetics. In the previous reports on hybridization kinetics, Wang et al observed that GC-rich toeholds lead to higher binding rates than AT-rich ones do by a factor of 15.[34] Similarly, Ouldridge et al revealed that a GC-rich sequence exhibits faster DNA-DNA hybridization than its AT-rich analog does by a factor of 7.4.[35] In our case, the sequence of let-7b had two fewer GC pairs (10 vs 8) and one more uracil (9 vs 8) than the sequence of miR-21 did. By considering both our experimental results and the sequence composition, it can be concluded that by slowing the hybridization kinetics, the uracil contributed more to reducing duplex stability and hybridization rates than the effect of the GC-rich sequence did, which is in agreement with the previous reports that DNA-DNA duplexes form faster than RNA-DNA heteroduplexes.[36] In addition, the observed hybridization time for the bulk solution was close to the shortest time reported for previous SPR platforms, showing that the DNA duplex could reach equilibrium in a period of time ranging from 3 min to several hours.[28]

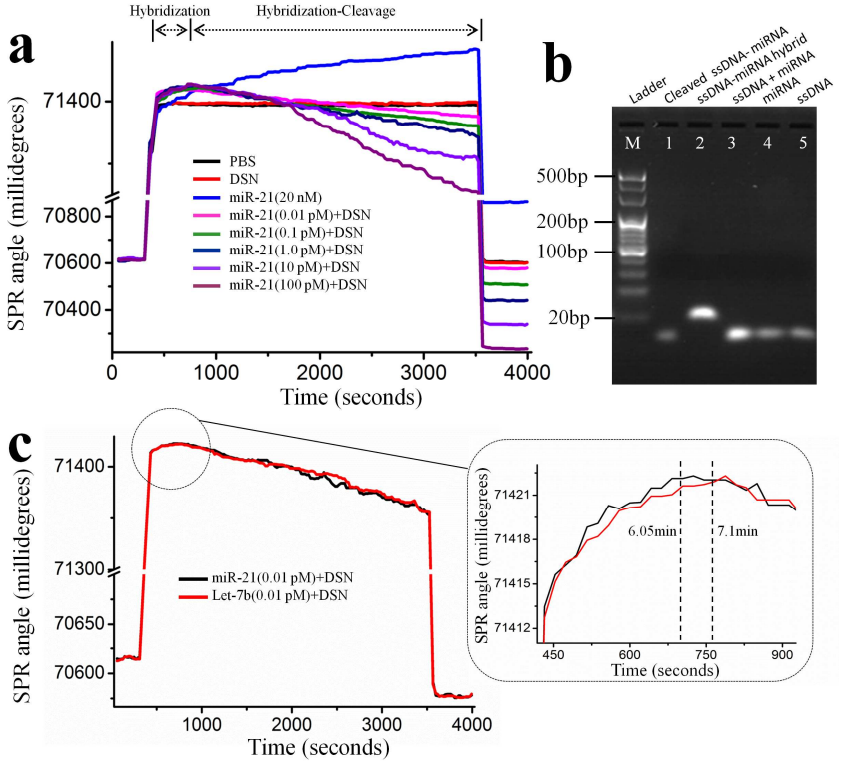

Figure 2. Dynamic monitoring of DSN-mediated cleavage of the miRNA-DNA hybrid. (a) Real-time recording of the processes of hybridization and cleavage in the DSN-SPR assay. The SPR angle changed upon addition of a series of miR-21 concentrations (0.01, 0.1, 1, 10, and 100 pM). (b) DSN-mediated cleavage of the ssDNA in the miRNA-DNA hybrid, as assessed by agarose gel electrophoresis. Lane M, 20 bp DNA ladder; Lane 1, product of 0.2 U DSN-cleaved miRNA-DNA hybrid; Lane 2, miRNA-DNA hybrid from 5 μM P-21 probe and 5 μM miR-21; Lane 3, mixture of 5 μM ssDNA P-21 probe and 5 μM target miR-21, without hybridization; Lane 4, 5 μM target miR-21; Lane 5, 5 μM ssDNA P-21 probe. (c) Comparison of hybridization rates between miR-21 and let-7b. The inset is an amplification of the circled part of the graph. miR-21 reached a peak at 6.05 min (black), and let-7b reached a maximum SPR angle shift at 7.1 min (red).

Characterization of rGO interface-induced probe coating. In the proposed label-free DSN-SPR assay, both the optimal probe-coating conditions and the hybridization buffer play critical roles in guaranteeing the analytical sensitivity and specificity. Because the SPR angle shift is proportional to the amount of hydrolyzed probe, the sensitivity of the proposed

assay is predominately dependent on the total amount of the immobilized probe. Conventional assays always require an optimized probe coating concentration to ensure the highest hybridization efficiency because both overcrowded and sparse probe densities would compromise the sensitivity.[37,38] However, the highest probe amounts available may be applied in the proposed assay because the trace target would preferentially hybridize to the peripheral probes if the coated probe array were overcrowded, such that the steric hindrance effect that frequently occurs in conventional assays could be substantially eliminated.[39]

To increase the amount of coated probes, rGO was deposited on the surface of the SPR biosensor chip because this substance can provide a higher surface-to-volume ratio than gold can, which is attributable to the π-stacking interactions between the carbon-based ring structures of biological molecules and the hexagonal cells of graphene.[40] Recently, such graphene-fabricated SPR chips have been theoretically and experimentally investigated for improving the sensitivity of conventional SPR biosensors.[41,42] It is believed that coating the gold surface with a dielectric film will change the power flow in different layers and modify the field of the surface plasmon polariton. Wu et al[43] showed that a graphene-on-gold SPR biosensor (with L graphene layers) is expected to be $(1 + 0.025\ L) \times \gamma$ times (γ: factor of increased adsorption efficiency) more sensitive than a conventional gold thin-film SPR biosensor. This increased sensitivity may be due to two properties of graphene: (a) Graphene strongly and stably adsorbs biomolecules with carbon-based ring structures, so graphene can be used as the biomolecular recognition element to enhance the adsorption efficiency by a factor of γ. (b) Graphene's optical property modifies the SPR curves and increases the sensitivity by 25% for $L = 10$. Moreover, Wang et al developed a graphene-modified SPR aptasensor for the detection of α-thrombin.[44] An improved detection limit was achieved using the graphene-coated gold interface to adsorb a significantly increased amount of aptamers. In the current study, to facilitate the fabrication of a graphene coating on the surface of gold, GO was reduced electrochemically by extended potential cycling (-1.24 to 0.76 V vs RHE, 50 mV s^{-1}) in 0.1 M Na_2SO_4. The results showed the typical reduction current peaks for GO at approximately -0.75 V and 0.1 V, suggesting successful electrochemical reduction of GO (Figure 3a).

The deposition of rGO on the SPR chip was further characterized by observing the Raman spectra of the electrochemically deposited rGO films. This characterization showed that the rGO films had two typical peaks, at ~1330 and ~1600 cm^{-1}, corresponding to the D and G modes of rGO, respectively (Figure 3b). A D-to-G intensity ratio of 1.43 was calculated after the electrochemical reduction, which may be attributable to the increased defect concentration in rGO compared with the defect concentration in GO.[45,46] SEM images showed that the rGO film had a more wrinkled and rougher surface than the gold film (Figure 3c), which could facilitate probe immobilization because electrolyte ions could more easily penetrate and diffuse in the rGO film.[47] In our experiments, the rGO modification provided a nearly 6-fold improvement in the immobilized probe density over traditional gold-modified SPR chips (~3×10^{12} molecules/cm^2 vs ~5×10^{11} molecules/cm^2) via electrowetting on dielectric (EWOD). The increased probe amounts were further verified by observing the induced SPR angle shift after deposition, which showed that the SPR angle shift was ~322 millidegrees stronger (~4.8 times higher if the blank is subtracted) for the rGO chip than for the bare gold chip (Figure 3d). This finding demonstrates the improved immobilization capability afforded by the rGO-modified SPR chip.

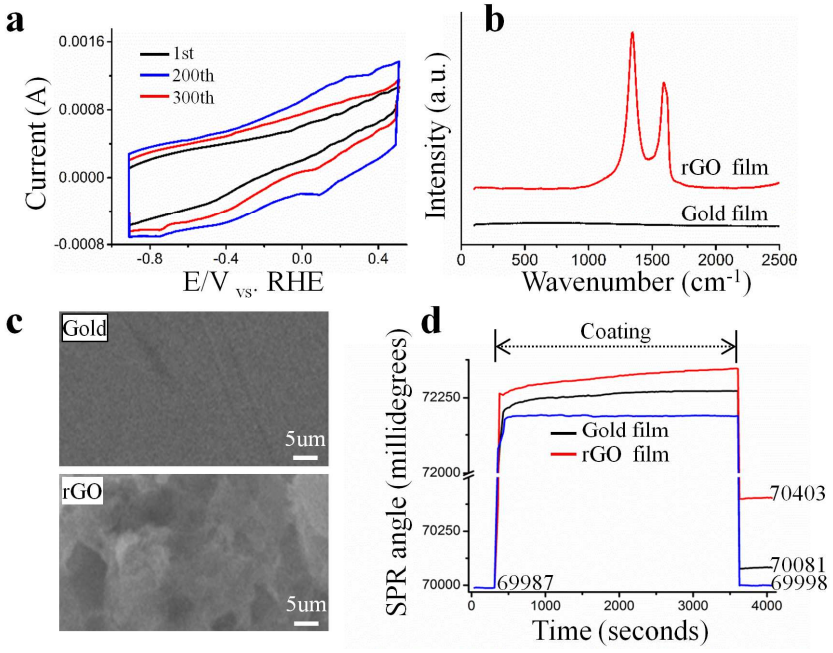

Figure 3. DNA probe immobilization on the rGO-modified SPR chip. (a) Cyclic voltammograms of the electrochemical reduction of GO in 0.1 M Na_2SO_4 at 50 mV s^{-1}. (b) Raman spectra of gold film (black) and rGO film (red). (c) SEM images of gold film (top) and rGO film

(bottom) coated on an SPR chip. Conditions: Vacc = 10 kV, Mag = ×10.0 k, WD = 9.1 mm. (d) SPR angle shift of the rGO-modified chip, induced by probe immobilization. The X-axis is the coating time, and the Y-axis is the SPR angle shift. In particular, the SPR angle shifts of the bare gold chip (black), the rGO chip (red), and the blank (blue) are shown.

Optimization of operating parameters. Because the presence of divalent cations such as manganese, cobalt or magnesium is required to ensure the desired cleavage activity, the Mg^{2+} ion concentration was optimized in this study. Our results show that a minimum concentration of 5 mM Mg^{2+} was needed for effective hydrolysis, and 20 mM was the optimal value.[48] We also optimized the working temperature because both the hybridization and the cleavage efficiencies would be affected by the temperature. A maximum SPR angle shift was observed at 50°C (the highest temperature possible for the apparatus), although higher temperatures may improve subsequent cleavage (Figure S1 in Supporting Information). In addition, 0.2 U DSN was observed to lead to the largest SPR angle shift in 50 μL of a solution containing 100 nM miRNA-DNA hybrid (Figure S2 in Supporting Information), which is similar to previously reported results.[49,50]

The operating characteristics of the proposed DSN-SPR assay for miR-21 quantification were investigated further. Our preliminary study showed that even the highest amount of P-21 probe could be cleaved completely within 60 min at an optimal DSN concentration of 0.2 U, when the target density was 100 pM. In addition, longer analytical times were found to be required for a lower concentration of the target to reach the reaction endpoint, which was manifested by a less sharp SPR angle shift. This result illustrates that the target miRNA concentration could be determined by plotting the target concentration against the analytical time (Figure 4a). We observed that the lowest target concentration (10 fM) yielded an SPR angle of 18.49 millidegrees at the endpoint (after approximately 60 min) following subtraction of the blank control. We set this endpoint as the benchmark to compare the analytical times needed for different target miRNA concentrations to reach this endpoint. Considering that all of the target solutions with higher concentrations required less time to reach the endpoint, all results were adjusted by setting the final SPR angle to 18.49 millidegrees, and the reaction time required was obtained accordingly (Figure 4a). Considering that DSN mediated a linear signal amplification, a linear model was employed to fit the working time (t) vs the target miR-21 concentration (C) using the calibration equation $t = -414\ x + 2309.7$, where t is the working time and x is the miR-21 concentration, over a linear range from 10 fM to 100 pM miR-21 and using a correlation coefficient of $R^2 = 0.987$ (Figure 4b). The detection limit of the rGO-modified SPR sensor was estimated to be 3 fM according to the 3σ rule, which is better than or comparable to the detection limits of several previously developed fluorescence assays for miRNA detection.[51,52] Notably, improved sensitivity to miR-21 concentrations could also be achieved by extending the analytical time to more than 60 min. The extraordinary sensitivity could be attributed to both the DSN-mediated linear signal amplification and the high capacity for biomolecule adsorption on the surface of the rGO-modified SPR chips.

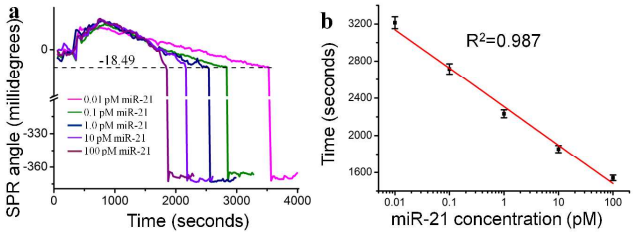

Figure 4. Calibration curve of the proposed DSN-SPR assay. (a) The SPR angle shifts upon addition of different concentrations of miR-21 (0.01, 0.1, 1, 10, and 100 pM) after subtracting the control value. The dotted line (-18.49 millidegrees) denotes the SPR angle shift induced by the lowest miR-21 concentration after subtracting the shift in the blank control. (b) The calibration curve of the DSN-SPR assay. The Y-axis is the reaction time, and the X-axis is the miR-21 concentration. Each error bar represents the standard error of three repeated tests.

Apart from the increased sensitivity, the specificity of the proposed DSN-SPR assay was validated by detecting different molecules (miR-143 and miR-141) with sequences similar to that of miR-21. No significant nonspecific adsorption on the rGO-based SPR chips was observed after blocking the chips with salmon sperm DNA (Figure S3 in Supporting Information). Additionally, 100 pM miR-143, 100 pM miR-141, and a blank control were observed to induce negligible SPR angle shifts, whereas 100 pM miR-21 produced a significant decrease in the SPR angle (by ~300 millidegrees). This finding suggested that the proposed assay can effectively differentiate miR-21 from other miRNAs in a P-21 probe-coated chip (Figure 5a). Similar results showed that 100 pM let-7b yielded a significant SPR angle shift in a let-7b probe-coated SPR chip, whereas miRNAs that differed by merely a few bases (let-7a, let-7c, and let-7e) could induce only extremely weak signals (Figure 5b), validating the excellent capability of DSN to distinguish perfectly matched miRNA-DNA hybrids from non-perfectly matched hybrids, including those with a single base mismatch.

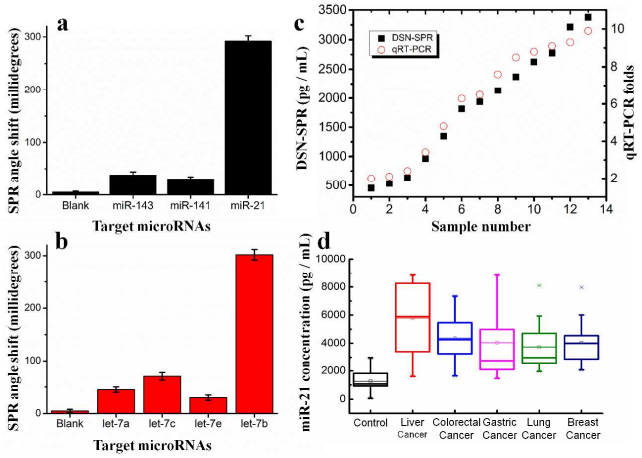

Figure 5. Specificity and clinical feasibility of the DSN-SPR assay. SPR angle shifts in the rGO-modified SPR chips coated by the miR-21 probe (a) or let-7b probe (b). The columns represent the SPR angle shift with different miRNA targets at a concentration of 10 pM. The error bars denote the standard errors of three repeated experiments. (c) Paired comparison of the miR-21 levels detected in 13 clinical blood samples using the proposed DSN-SPR assay (black square) or qRT-PCR (red circle). (d) Validation of the capability of differentiating the miR-21 concentration in 20 control samples (black) from that in liver cancer (red), colorectal cancer (blue), gastric cancer (pink), lung cancer (green), and breast cancer (brown). The asterisks denote the 99% and 1% percentiles, and the hollow square denotes the mean of the total samples.

The accuracy of the developed DSN-SPR approach was tested by calculating the recoveries of known amounts of miR-21 or let-7b spiked into blood samples, and satisfactory recovery rates for standard addition, ranging from 94.1% to 107.3%, were obtained (Table S1 in Supporting Information). The relative expression levels of miR-21 in 13 serum samples were specifically determined using both qRT-PCR and the proposed DSN-SPR assay. The results showed that these levels ranged from 70 pg/mL to 3400 pg/mL (Figure 5c), corresponding to fold differences from qRT-PCR that ranged from 2-fold to 10-fold, revealing good consistency between the DSN-SPR and the qRT-PCR assays. To determine the feasibility of applying the proposed assay to real biological samples, circulating miR-21 was detected in blood samples from 100 inpatients, including breast cancer, lung cancer, and liver cancer patients. The results showed that the miR-21 concentrations in the control group were significantly lower than the miR-21 concentrations in these cancer patients (Figure 5d), suggesting that the proposed DSN-SPR assay can effectively differentiate between various cancers.

CONCLUSION

In this paper, we reported the first approach for dynamic monitoring of miRNA-DNA hybridization and DSN-mediated cleavage in a direct, single-step manner. The proposed DSN-SPR assay is advantageous because it integrates the exclusive hydrolytic capability of DSN and the real-time monitoring feature of an SPR biosensor. Moreover, miRNAs could be quantified in a rapid and ultrasensitive manner due to the extraordinary capability of rGO-enabled DNA probes immobilized on SPR chips. As it does not require complicated procedures or sophisticated instrumentation, the proposed assay is promising for the design of multiplex miRNA-profiling strategies that simply employ different types of ssDNA probes.

AUTHOR INFORMATION

Corresponding Author

* Tel.: 86-23-68765485. Fax: 86-23-68765986. E-mail: luoyang@tmmu.edu.cn

Author Contributions

#These authors contributed equally.

Notes

The authors declare no competing financial interest.

ACKNOWLEDGMENTS

This work was supported by the National Natural Science Foundation of China (81371899); the Science Fund for Distinguished Young Scholars (CSTC2014JCYJJQ10007); the Natural Science Foundation of Chongqing, China (CSTC2013JJB10012); the Twelfth Five-Year Plan of PLA, China (CWS13C046); the China Academy of Engineering Physics (WSS-2014-09); and the Third Military Medical University of China (SWH2013LC13).

ASSOCIATED CONTENT

Supporting Information

Additional information is provided, as noted in the text. This material is available free of charge via the Internet at http://pubs.acs.org.

REFERENCES

(1) Bartel, D. P. *Cell* **2009**, *136*, 215-233.

(2) Schwarzenbach, H.; Nishida, N.; Calin, G. A.; Pantel, K. *Nature reviews. Clinical oncology* **2014**, *11*, 145-156.

(3) Mitchell, P. S.; Parkin, R. K.; Kroh, E. M.; Fritz, B. R.; Wyman, S. K.; Pogosova-Agadjanyan, E. L.; Peterson, A.; Noteboom, J.; O'Briant, K. C.; Allen, A.; Lin, D. W.; Urban, N.; Drescher, C. W.; Knudsen, B. S.; Stirewalt, D. L.; Gentleman, R.; Vessella, R. L.; Nelson, P. S.; Martin, D. B.; Tewari, M. *Proc Natl Acad Sci* **2008**, *105*, 10513-10518.

(4) Cheng, G. F. *Adv Drug Delivery Rev* **2015**, *81*, 75-93.

(5) Pritchard, C. C.; Cheng, H. H.; Tewari, M. *Nat Rev Genet* **2012**, *13*, 358-369.

(6) Turchinovich, A.; Weiz, L.; Langheinz, A.; Burwinkel, B. *Nucleic Acids Res* **2011**, *39*, 7223-7233.

(7) Raymond, C. K.; Roberts, B. S.; Garrett-Engele, P.; Lim, L. P.; Johnson, J. M. *Rna* **2005**, *11*, 1737-1744.

(8) Li, J.; Yao, B.; Huang, H.; Wang, Z.; Sun, C.; Fan, Y.; Chang, Q.; Li, S.; Wang, X.; Xi, J. *Anal Chem* **2009**, *81*, 5446-5451.

(9) Tam, S.; de Borja, R.; Tsao, M. S.; McPherson, J. D. *Lab Invest* **2014**, *94*, 350-358.

(10) Silahtaroglu, A. N.; Nolting, D.; Dyrskjot, L.; Berezikov, E.; Moller, M.; Tommerup, N.; Kauppinen, S. *Nature Protocols* **2007**, *2*, 2520-2528.

(11) Varallyay, E.; Burgyan, J.; Havelda, Z. *Nature Protocols* **2008**, *3*, 190-196.

(12) Chen, Y. X.; Gelfond, J. A. L.; McManus, L. M.; Shireman, P. K. *Bmc Genomics* **2009**, *10*, 407.

(13) Lim, L. P.; Lau, N. C.; Garrett-Engele, P.; Grimson, A.; Schelter, J. M.; Castle, J.; Bartel, D. P.; Linsley, P. S.; Johnson, J. M. *Nature* **2005**, *433*, 769-773.

(14) Nelson, P. T.; Baldwin, D. A.; Scearce, L. M.; Oberholtzer, J. C.; Tobias, J. W.; Mourelatos, Z. *Nature methods* **2004**, *1*, 155-161.

(15) Git, A.; Dvinge, H.; Salmon-Divon, M.; Osborne, M.; Kutter, C.; Hadfield, J.; Bertone, P.; Caldas, C. *Rna* **2010**, *16*, 991-1006.

(16) Qiu, X.; Zhang, H.; Yu, H.; Jiang, T.; Luo, Y. *Trends Biotechnol* **2015**, *33*, 180-188.

(17) Shagin, D. A.; Rebrikov, D. V.; Kozhemyako, V. B.; Altshuler, I. M.; Shcheglov, A. S.; Zhulidov, P. A.; Bogdanova, E. A.; Staroverov, D. B.; Rasskazov, V. A.; Lukyanov, S. *Genome Res* **2002**, *12*, 1935-1942.

(18) Yin, B. C.; Liu, Y. Q.; Ye, B. C. *J Am Chem Soc* **2012**, *134*, 5064-5067.

(19) Deng, H. M.; Ren, Y. Q.; Shen, W.; Gao, Z. Q. *Chem Commun* **2013**, *49*, 9401-9403.

(20) Ren, Y. Q.; Deng, H. M.; Shen, W.; Gao, Z. Q. *Anal Chem* **2013**, *85*, 4784-4789.

(21) Wang, S.; Fu, B.; Wang, J.; Long, Y.; Zhang, X.; Peng, S.; Guo, P.; Tian, T.; Zhou, X. *Anal Chem* **2014**, *86*, 2925-2930.
(22) Tian, T.; Xiao, H.; Zhang, Z. G.; Long, Y. L.; Peng, S.; Wang, S. R.; Zhou, X.; Liu, S. M.; Zhou, X. *Chem-Eur J* **2013**, *19*, 92-95.
(23) Szunerits, S.; Maalouli, N.; Wijaya, E.; Vilcot, J. P.; Boukherroub, R. *Anal Bioanal Chem* **2013**, *405*, 1435-1443.
(24) Iorio, M. V.; Ferracin, M.; Liu, C. G.; Veronese, A.; Spizzo, R.; Sabbioni, S.; Magri, E.; Pedriali, M.; Fabbri, M.; Campiglio, M.; Menard, S.; Palazzo, J. P.; Rosenberg, A.; Musiani, P.; Volinia, S.; Nenci, I.; Calin, G. A.; Querzoli, P.; Negrini, M.; Croce, C. M. *Cancer Res* **2005**, *65*, 7065-7070.
(25) Asaga, S.; Kuo, C.; Nguyen, T.; Terpenning, M.; Giuliano, A. E.; Hoon, D. S. *Clin Chem* **2011**, *57*, 84-91.
(26) Menendez, P.; Padilla, D.; Villarejo, P.; Palomino, T.; Nieto, P.; Menendez, J. M.; Rodriguez-Montes, J. A. *J Surg Oncol* **2013**, *108*, 369-373.
(27) Ke, Y.; Lindsay, S.; Chang, Y.; Liu, Y.; Yan, H. *Science* **2008**, *319*, 180-183.
(28) Gao, Y.; Wolf, L. K.; Georgiadis, R. M. *Nucleic Acids Res* **2006**, *34*, 3370-3377.
(29) Wegman, D. W.; Krylov, S. N. *Trac-trend in Anal Chem* **2013**, *44*, 121-130.
(30) Schwille, P.; Oehlenschlager, F.; Walter, N. G. *Biochemistry-us* **1996**, *35*, 10182-10193.
(31) Wong, E. L.; Chow, E.; Gooding, J. J. *Langmuir* **2005**, *21*, 6957-6965.
(32) Stillman, B. A.; Tonkinson, J. L. *Anal Biochem* **2001**, *295*, 149-157.
(33) Tawa, K.; Yao, D.; Knoll, W. *Biosens Bioelectron* **2005**, *21*, 322-329.
(34) Zhang, D. Y.; Winfree, E. *J Am Chem Soc* **2009**, *131*, 17303-17314.
(35) Ouldridge, T. E.; Sulc, P.; Romano, F.; Doye, J. P.; Louis, A. A. *Nucleic Acids Res* **2013**, *41*, 8886-8895.
(36) Rauzan, B.; McMichael, E.; Cave, R.; Sevcik, L. R.; Ostrosky, K.; Whitman, E.; Stegemann, R.; Sinclair, A. L.; Serra, M. J.; Deckert, A. A. *Biochemistry-us* **2013**, *52*, 765-772.
(37) Mirnaghi, F. S.; Chen, Y.; Sidisky, L. M.; Pawliszyn, J. *Anal Chem* **2011**, *83*, 6018-6025.
(38) Yiu, H. H.; Bouffier, L.; Boldrin, P.; Long, J.; Claridge, J. B.; Rosseinsky, M. J. *Langmuir* **2013**, *29*, 11354-11365.
(39) Michel, W.; Mai, T.; Naiser, T.; Ott, A. *Biophys J* **2007**, *92*, 999-1004.
(40) Subramanian, P.; Lesniewski, A.; Kaminska, I.; Vlandas, A.; Vasilescu, A.; Niedziolka-Jonsson, J.; Pichonat, E.; Happy, H.; Boukherroub, R.; Szunerits, S. *Biosens Bioelectron* **2013**, *50*, 239-243.
(41) Mao, Y.; Bao, Y.; Wang, W.; Li, Z.; Li, F.; Niu, L. *Talanta* **2011**, *85*, 2106-2112.
(42) Szunerits, S.; Maalouli, N.; Wijaya, E.; Vilcot, J. P.; Boukherroub, R. *Anal Bioanal Chem* **2013**, *405*, 1435-1443.
(43) Wu, L.; Chu, H. S.; Koh, W. S.; Li, E. P. *Opt Express* **2010**, *18*, 14395-14400.
(44) Wang, L.; Zhu, C.; Han, L.; Jin, L.; Zhou, M.; Dong, S. *Chem Commun (Camb)* **2011**, *47*, 7794-7796.
(45) Stankovich, S.; Dikin, D. A.; Piner, R. D.; Kohlhaas, K. A.; Kleinhammes, A.; Jia, Y.; Wu, Y.; Nguyen, S. T.; Ruoff, R. S. *Carbon* **2007**, *45*, 1558-1565.
(46) Ramesha, G. K.; Sampath, S. *J Phys Chem C* **2009**, *113*, 7985-7989.
(47) Zhang, X.; Zhang, D.; Chen, Y.; Sun, X.; Ma, Y. *Chinese Science Bulletin* **2012**, *57*, 3045-3050.
(48) Anisimova, V. E.; Rebrikov, D. V.; Shagin, D. A.; Kozhemyako, V. B.; Menzorova, N. I.; Staroverov, D. B.; Ziganshin, R.; Vagner, L. L.; Rasskazov, V. A.; Lukyanov, S. A.; Shcheglov, A. S. *Bmc Biochem* **2008**, *9*, 14.
(49) Xi, Q.; Zhou, D. M.; Kan, Y. Y.; Ge, J.; Wu, Z. K.; Yu, R. Q.; Jiang, J. H. *Anal Chem* **2014**, *86*, 1361-1365.
(50) Qiu Xiaopei, Z. H., Jiang Tianlun, Luo Yang. *Progress in Chemistry* **2014**, *26*, 840-1848.
(51) Guo, S.; Yang, F.; Zhang, Y. L.; Ning, Y.; Yao, Q. F.; Zhang, G. J. *Anal Methods-UK* **2014**, *6*, 3598-3603.
(52) Degliangeli, F.; Kshirsagar, P.; Brunetti, V.; Pompa, P. P.; Fiammengo, R. *J Am Chem Soc* **2014**, *136*, 2264-2267.

For TOC only

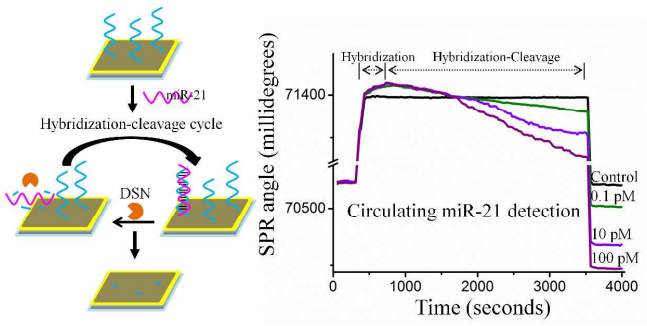
miR-21
Hybridization-cleavage cycle
DSN
Hybridization
Hybridization-Cleavage
71400
70500
SPR angle (millidegrees)
Circulating miR-21 detection
Control
0.1 pM
10 pM
100 pM
0
1000
2000
3000
4000
Time (seconds)